Petroleum Science 23 (2026) 680–691

Contents lists available at ScienceDirect

Petroleum Science

journal homepage: www.keaipublishing.com/en/journals/petroleum-science

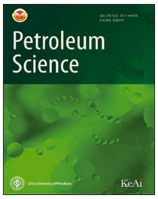

Original Paper

A novel NMR methodology for the quantitative characterization of solid organic matter in shale oil

Chen-Yu Xu [a,b], Ran-Hong Xie [a,b,*], Jiang-Feng Guo [a,b], Xiang-Yu Wang [a,b], Li-Zhi Xiao [a,b], Guo-Wen Jin [a,b], Bo-Chuan Jin [a,b], Xiao-Long Ju [a,b]

[a] State Key Laboratory of Petroleum Resources and Engineering, China University of Petroleum (Beijing), Beijing, 102249, China
[b] Key Laboratory of Earth Prospecting and Information Technology, China University of Petroleum (Beijing), Beijing, 102249, China

ARTICLE INFO

Article history:
Received 22 June 2025
Received in revised form
24 August 2025
Accepted 4 November 2025
Available online 8 November 2025

Edited by Meng-Jiao Zhou

Keywords:
Shale oil reservoir
Solid organic matter
Nuclear magnetic resonance
Free induction decay
T_1-T_2^* spectra

ABSTRACT

Continental shale oil reservoirs in China, particularly those of low to medium maturity, contain a high proportion of untransformed solid organic matter (SOM). The SOM plays a critical role as a potential oil and gas resource. Nuclear magnetic resonance (NMR) is a powerful technique for the evaluation of shale oil reservoirs. However, it is challenging for conventional T_1-T_2 measurement methods to fully capture signals from ultra-short relaxation components such as SOM, due to the measurement deficiency caused by NMR instruments. To this end, the free induction decay (FID) and inversion recovery FID (IR-FID) pulse sequences are introduced, and two novel methods are proposed for quantitative characterization of SOM. The first method, Method I, employs the signal amplitude difference between T_2^* and T_1-T_2 spectra to obtain the SOM content. The second, Method II, directly quantifies the SOM signal from the T_1-T_2^* spectrum. A novel parameter, the ratio of T_1/T_2^* to T_1/T_2, is also proposed to refine the identification of SOM in the T_1-T_2 spectrum. The effectiveness of the proposed methods is validated by strong correlations with four geochemical parameters indicative of SOM content. The results from Method I show significantly improved correlations with all four geochemical parameters compared to the conventional T_1-T_2 method. The results from Method II show excellent correlations with parameters from step-by-step (SBS) Rock-Eval pyrolysis, reaching coefficients of determination (R^2) as high as 0.8958 and 0.8828. This method also shows strong numerical consistency with the geochemical parameters, specifically with ($S_{1-2b} + S_{2-1}+S_{2-2}$). Method II is therefore highly suitable for quantitatively evaluating the total solid hydrogen content, including solid petroleum hydrocarbons, bitumen, and kerogen. This work achieves, for the first time, the precise quantification of SOM at the core scale, providing a high-precision, large-scale, and non-destructive approach for evaluating the resource potential of shale oil reservoirs.

1. Introduction

Conventional oil and gas resources face the dual challenges of declining production and the diminishing quality of newly discovered reservoirs, amid the continued development of China's national economy and the rising demand for energy (Yang and Jin, 2019; Zou et al., 2020, 2023). Shale oil is regarded as a highly promising alternative energy resource, owing to its substantial reserves and widespread distribution (Yang and Zou, 2019; Jia et al., 2018a). The majority of continental shale oil resources are at a low to medium maturity stage in China. The proportion of unconverted solid organic matter (SOM) is notably high, accounting for 40%–80% of the total organic content (Zhao et al., 2020; Zou et al., 2013). This SOM holds considerable potential for conversion into movable oil and gas resources through in-situ underground heating technologies (Zhao et al., 2020; Hu et al., 2020). Therefore, the quantitative characterization of SOM in shale oil reservoirs is instrumental in accurately assessing reservoir resource potential and optimizing development strategies, which is the key to ensuring national energy security.

---

* Corresponding author.
E-mail address: xieranhong@cup.edu.cn (R.-H. Xie).

Peer review under the responsibility of China University of Petroleum (Beijing).

https://doi.org/10.1016/j.petsci.2025.11.009

Currently, quantitative characterization of SOM in shale oil reservoirs predominantly relies on geochemical laboratory methods, particularly solvent extraction and Rock-Eval pyrolysis. The solvent extraction method is employed to separate soluble bitumen from SOM. The remaining extraction residue subsequently undergoes acid and base treatment to isolate the insoluble kerogen fraction. This sequential process enables quantitative characterization of both bitumen and kerogen within the SOM (Xie et al., 2016; Qian et al., 2017). However, this method entails cumbersome and time-consuming procedures and cannot reliably ensure efficient bitumen extraction or effective component separation. Routine Rock-Eval pyrolysis involves heating core samples to quantify free hydrocarbons and cracking hydrocarbons. The cracking hydrocarbons, originating mainly from the heavy hydrocarbons, bitumen, and kerogen, are a commonly used geochemical proxy for SOM content. Although this method is relatively straightforward in operation, its accuracy in SOM quantification is susceptible to several factors. For instance, "carry-over" effects and confinement phenomena during pyrolysis can lead to signal overlap among different hydrocarbon types. Furthermore, incomplete thermal conversion of SOM under programmed heating conditions can also compromise the accuracy of quantitative characterization (Peters, 1986; Romero-Sarmiento, 2019). The step-by-step (SBS) Rock-Eval pyrolysis method, developed in recent years, employs more refined temperature programming. This refinement enhances the resolution and characterization accuracy for different hydrocarbon fractions (Jiang et al., 2016; Zhang et al., 2020; Li et al., 2020). Despite these advancements, the SBS Rock-Eval method still requires sample pulverization and is constrained by a limited observation scale. These inherent limitations restrict its applicability for meeting practical demands of rapid, non-destructive SOM characterization in shale oil reservoirs.

Nuclear magnetic resonance (NMR) is a non-destructive technology used to acquire key reservoir parameters, including porosity, permeability, and saturation, by detecting the resonance of hydrogen nuclei within a magnetic field. This technique has been widely applied in oil and gas exploration (Song and Kausik, 2019; Jin et al., 2020; Gu et al., 2021). The measurement of transverse relaxation time (T_2) is currently predominantly performed using the Carr-Purcell-Meiboom-Gill (CPMG) pulse sequence. However, this technique is constrained by the minimum echo spacing (TE), typically 60–600 μs, achievable with laboratory or logging instruments. Consequently, signals from components with short relaxation times in shale, particularly SOM, decay substantially before the instrument initiates signal acquisition, resulting in SOM content underestimation. Extensive research has been conducted to capture this missing signal. Early studies introduced more complex pulse sequences, such as Solid-Echo and Magic-Echo, to recover the signals from short-relaxation components (Washburn and Birdwell, 2014; Jia et al., 2018a, 2018b; Liu et al., 2023). However, these approaches involve complex sequence editing and data processing and typically require stringent instrument hardware and experimental conditions. In recent years, advances in NMR instrumentation have significantly reduced the impact of magnetic field inhomogeneity on T_2^* measurements using free induction decay (FID) pulse sequences. Modern laboratory low-field NMR instruments now feature dead times of only tens of microseconds and acquisition time steps as short as nanoseconds, enabling effective capture of signals from ultra-short relaxation components. This technology has been successfully applied to characterize short-relaxation signals in various other systems containing solid components, including flour, cement, polymers, and coal powder (Rondeau-Mouro et al., 2016; Enjileala et al., 2021; Guo et al., 2021a, 2021b). FID-based measurements have also been employed for shale sample measurements, with multiple studies confirming that FID pulse sequence can detect substantially more short-relaxation component signals than CPMG pulse sequence (Zamiri et al., 2021, 2022; Silletta et al., 2022; Guo et al., 2022). Among these, the recent work of Xu et al. (2024) demonstrated that the signal amplitude difference between T_2^* spectra (from FID) and T_2 spectra (from CPMG) can effectively predict geochemical parameters such as total organic carbon (TOC), confirming a high correlation between the additionally detected FID signal and SOM content. A significant challenge in quantifying SOM using 1D NMR (T_2^* and T_2 spectra) is the signal overlap from other components with similarly ultra-short relaxation times, namely hydrocarbons with low-mobility and clay-bound water. This spectral interference makes effective separation difficult and leads to an overestimation of the SOM content. Two-dimensional (2D) NMR measurement methods, such as T_1-T_2 and T_1/T_2-T_2 spectrum, have recently gained increasing prominence in the evaluation of shale oil reservoirs, offering richer insights into fluid components, wettability, and mobility (Fleury and Romero-Sarmiento, 2016; Kausik et al., 2016; Li et al., 2020; Mukhametdinova et al., 2021; Xu et al., 2023). However, since these powerful 2D methods are typically based on the CPMG sequence, they inherit the same fundamental limitation of underestimating SOM content. Furthermore, few studies have applied FID-based 2D NMR techniques to the quantification of SOM.

In this paper, two novel methods are proposed for the quantitative characterization of SOM in shale reservoirs. The first approach, Method I, utilizes the signal amplitude difference between T_2^* and T_1-T_2 spectra to determine the SOM content. The second, Method II, employs an innovative parameter, the ratio of $(T_1/T_2^*)/(T_1/T_2)$, to distinguish the SOM signal in T_1-T_2^* spectrum before quantifying its content based on signal amplitude. The effectiveness of the proposed methods is systematically validated against key geochemical indicators from TOC analysis and Rock-Eval pyrolysis. Ultimately, this work aims to establish a non-destructive and precise methodology for SOM characterization at the core scale, providing a more accurate tool to assess the full resource potential of shale reservoirs and guide the deployment of in-situ conversion technologies.

2. Methodology

2.1. Theory

The relaxation of hydrogen nuclei (^{1}H) after radiofrequency (RF) excitation provides key information about fluid composition and pore structure in NMR analysis for shale. This study focuses on two relaxation mechanisms: longitudinal (spin-lattice) relaxation, characterized by the time constant T_1, and transverse (spin-spin) relaxation. Transverse relaxation can be described by two different time constants. The intrinsic spin-spin relaxation time, T_2, is typically measured using the CPMG pulse sequence as shown in Fig. 1(a). The CPMG sequence uses a train of 180° pulses to refocus signal decay caused by static magnetic field inhomogeneity. However, in the presence of such inhomogeneities, the observed signal decay is much faster, a phenomenon captured by the FID sequence and characterized by the effective transverse relaxation time, T_2^*, as shown in Fig. 1(b). The relationship between these constants is given by (Mitchell, 2014):

$$\frac{1}{T_2{}^*} \approx \frac{1}{T_2} + \gamma \Delta B_0 + \gamma \Delta \chi B_0 \quad (1)$$

Here, γ is the gyromagnetic ratio and ΔB_0 represents the

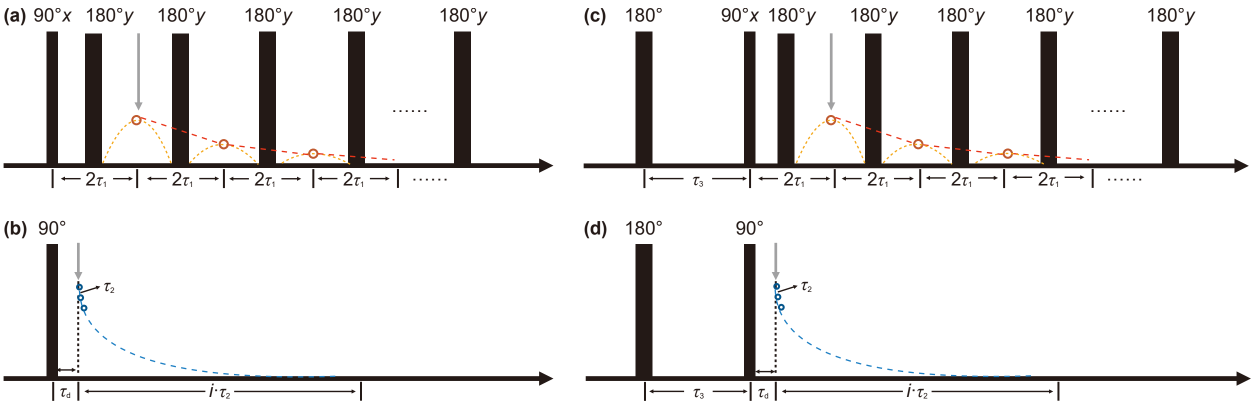

Fig. 1. Schematic diagrams of **(a)** CPMG, **(b)** FID, **(c)** IR-CPMG, and **(d)** IR-FID pulse sequences.

inhomogeneity of the magnetic field. In porous media like shale, significant field gradients are induced by the magnetic susceptibility difference, $\Delta\chi$, between pore fluids and the solid matrix (minerals and solid organic matter, SOM). This effect causes hydrogen in or near solid surfaces, particularly within SOM, to exhibit extremely short T_2^* values.

2.2. Pulse sequences

The ability to detect these ultra-short relaxation components is critically dependent on the pulse sequence's timing parameters. Conventional CPMG sequences are limited by a first TE that is typically between 60 and 100 μs for laboratory NMR instruments. This long initial delay prevents the detection of signals that decay faster than TE, leading to a significant underestimation of solid-like components such as SOM.

In contrast, the FID sequence offers a decisive advantage. Its instrument dead time (τ_d) can be as short as 20 μs or less, allowing it to capture the initial, rapidly decaying part of the signal that is completely missed by CPMG. This capability makes FID-based measurements uniquely suited for the direct characterization of SOM.

These measurements are combined within 2D experiments for comprehensive characterization. Through the integration of an IR pulse sequence, T_1-T_2 spectra are acquired with the IR-CPMG sequence, as shown in Fig. 1(c). T_1-T_2^* spectra are obtained using the IR-FID sequence as shown in Fig. 1(d). Since the T_1 encoding part of both sequences is identical, any difference in the resulting 2D spectra is directly attributable to the distinct between the T_2 and T_2^* transverse relaxation measurements. This fundamental distinction forms the basis of our novel methodology for identifying and quantifying SOM.

2.3. Identification of gaseous hydrocarbons using the $(T_1/T_2^*)/(T_1/T_2)$ ratio

When T_1-T_2 and T_1-T_2^* measurements are performed on the same shale sample with identical acquisition parameters during the T_1 recovery process, the NMR response of a specific hydrogen component in shale satisfies:

$$\frac{(T_1/T_2{}^*)}{(T_1/T_2)} \approx \frac{T_2}{T_2{}^*} = 1 + T_2\gamma(\Delta B_0 + \Delta\chi B_0) \tag{2}$$

Considering the influence of magnetic susceptibility differences $\Delta\chi$, Eq. (2) can be further expressed as:

$$\frac{(T_1/T_2{}^*)}{(T_1/T_2)} \approx 1 + T_2\gamma[\Delta B_0 + (\chi_\mathrm{H} - \chi_\mathrm{m})B_0] \tag{3}$$

where χ_H represents the magnetic susceptibility of the hydrogen component, and χ_m denotes the magnetic susceptibility of the mineral matrix. The presence of strongly paramagnetic minerals, such as pyrite, within the matrix is the primary source of this contrast, creating a pervasive background magnetic field gradient throughout the porous medium.

Crucially, the T_2 term in Eq. (3) is the intrinsic transverse relaxation time, a property governed by the molecular mobility of a given hydrogen component. Different components in shale exhibit vastly different intrinsic T_2 values. For instance, SOM, with its rigidly bound protons, exhibits an extremely short intrinsic T_2 in the order of microseconds. Hydrocarbons with low mobility have a short T_2 in the low millisecond range. In contrast, hydrocarbons with high mobility such as light oils and gas possess long T_2 values, ranging from ones to hundreds of milliseconds.

Eq. (3) thus reveals the underlying physical mechanism whereby the $(T_1/T_2^*)/(T_1/T_2)$ ratio leverages a component's intrinsic T_2 values as an amplifier for the effect of the static gradient. The significant differences in the intrinsic T_2 values lead to a clear hierarchy in the resulting ratio. This relationship can be expressed as:

$$\frac{(T_1/T_2{}^*)}{(T_1/T_2)}_\mathrm{SOM} < \frac{(T_1/T_2{}^*)}{(T_1/T_2)}_\mathrm{low\text{-}mobility} = \frac{(T_1/T_2{}^*)}{(T_1/T_2)}_\mathrm{high\text{-}mobility/gas} \tag{4}$$

where the subscripts represent different hydrogen components: the subscript "SOM" stands for solid organic matter, "low-mobility" for hydrocarbons with low mobility, "high-mobility" for hydrocarbons with high mobility, and "gas" for gaseous hydrocarbons.

This contrast provides a reliable basis for distinguishing between SOM and gaseous hydrocarbons, particularly within the conventional T_1-T_2 spectrum where the signal from gaseous hydrocarbons is fully captured.

2.4. Method I: SOM quantification based on T_2^* spectrum correction

Fig. 2 displays the T_1-T_2 spectrum for different hydrogen components in shale oil reservoirs. Peak A is generally considered to represent SOM. Peaks B, C, and D correspond to hydrocarbons with low mobility I, hydrocarbons with high mobility, and hydrocarbons with low mobility II, respectively. Peak E represents a mixed

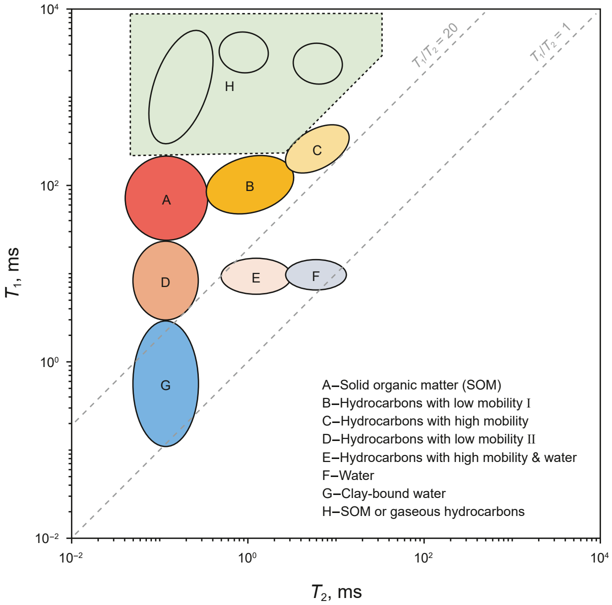

Fig. 2. T_1-T_2 spectrum showing characteristic regions for different hydrogen components in shale oil reservoirs.

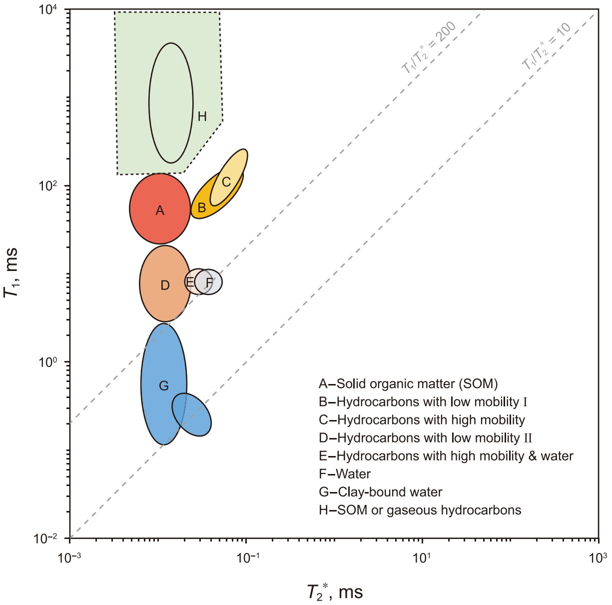

Fig. 3. T_1-T_2^* spectrum showing characteristic regions for different hydrogen components in shale oil reservoirs.

fluid phase of hydrocarbons with high mobility and water. Peak F denotes free water, and Peak G indicates clay-bound water. Peak H, characterized by a high T_1 value and short T_2 response, can represent either SOM or gaseous hydrocarbons. The latter can be identified using the $(T_1/T_2^*)/(T_1/T_2)$ Ratio. An initial estimation of the SOM content in shale oil core samples can be obtained by integrating the signal amplitudes of Peak A, or both Peak A and Peak H, from the T_1-T_2 spectrum.

As established previously, this conventional estimation is inherently incomplete because T_1-T_2 measurements fail to detect the full signal from ultra-short relaxation components. Method I is proposed to addresses this deficiency by using the comprehensive signal from a T_2^* spectrum to correct the T_1-T_2 spectrum. This approach operates on the key assumption that the signal lost by the IR-CPMG sequence is entirely attributable to undetected SOM. Therefore, a corrected SOM signal amplitude is calculated by adding this signal deficit to the originally measured SOM amplitude as described by the following equation:

$$\phi_{\mathrm{OM,corr}} = \phi_{t,T_2^*} - \phi_{t,T_1-T_2} + \phi_{\mathrm{OM},T_1-T_2} \tag{5}$$

where $\phi_{\mathrm{OM,corr}}$ represents the SOM content obtained after correcting the T_1-T_2 spectrum, ϕ_{t,T_2^*} is the total hydrogen content derived from the T_2^* spectrum, ϕ_{t,T_1-T_2} is the total hydrogen content derived from the T_1-T_2 spectrum, and $\phi_{\mathrm{OM},T_1-T_2}$ is the SOM content obtained from the T_1-T_2 spectrum.

2.5. Method II: SOM identification and quantification via T_1-T_2^* spectrum

Fig. 3 presents the T_1-T_2^* spectrum for different hydrogen components in shale oil reservoirs. In this spectrum, the signal of SOM primarily appears in regions corresponding to peak A and peak H, and it is comprehensively captured by the IR-FID sequence. However, the SOM signal in the Peak H region is susceptible to interference from gaseous hydrocarbons due to the influence of magnetic field inhomogeneity.

This interference is eliminated through a systematic correction. The final SOM content $\phi_{\mathrm{OM},T_1-T_2^*}$ is calculated using the following equation:

$$\phi_{\mathrm{OM},T_1-T_2^*} = A_{\mathrm{region},T_1-T_2^*} - A_{\mathrm{gas},T_1-T_2} \tag{6}$$

where $A_{\mathrm{region},T_1-T_2^*}$ represents the total signal amplitude integrated from the SOM region in the T_1-T_2^* spectrum, A_{gas,T_1-T_2} is the signal amplitude of gaseous hydrocarbons determined in T_1-T_2 spectrum.

3. Experimental

3.1. Materials

The Chang 7 Member of the Triassic Yanchang Formation in the Ordos Basin hosts a suite of organic-rich lacustrine black shales. These shales are characterized by exceptionally high organic matter abundance, moderate thermal maturity, and strong hydrocarbon generation potential, representing one of the primary source rock intervals in the Ordos Basin (Zhao et al., 2023). X-ray diffraction (XRD) analysis was performed on ten representative samples, as shown in Table 1. The results show that the mineral composition is dominated by silicate minerals and clay minerals, with average contents of 44.47% and 44.34%, respectively. Carbonate minerals and pyrite are present in smaller quantities, with average contents of 7.66% and 3.54%.

In this work, twenty as-received shale samples from this interval were selected for laboratory analysis. Each sample was divided into two parallel sets. One set was prepared as core plugs for NMR measurements, and the other was ground into powder for geochemical analyses, including total organic carbon (TOC) content determination, routine Rock-Eval pyrolysis, and SBS Rock-Eval pyrolysis.

3.2. NMR measurements

All NMR experiments were conducted using a MesoMR23-060H-I low-field NMR analyzer. The instrument operates at a ^{1}H

Table 1
Mineralogical composition of the representative shale samples determined by XRD analysis. Note: Q: Quartz; K: K-feldspar; PL: Plagioclase; C: Calcite; D: Dolomite; S: Siderite; PY: Pyrite; CM: Clay minerals; I/S: Illite/Smectite mixed-layer; I: Illite; K: Kaolinite; C: Chlorite.

Sample ID	Q, %	K, %	PL, %	C, %	D, %	S, %	PY, %	CM, %	I/S, %	I, %	K, %	C, %
#26	41.4	1.9	9.2	/	/	/	3.1	44.4	31	48	11	10
#28	31.6	4.2	9.8	/	2.7	/	3.4	48.3	52	32	8	8
#30	38.3	4.0	7.4	/	3.8	/	0.9	45.6	44	38	9	9
#31	37.8	1.3	1.9	/	1.0	/	4.6	53.4	34	50	10	6
#32	32.8	4.9	8.7	/	4.7	10.7	1.7	36.5	39	46	8	7
#34	31.9	13	7.7	/	2.1	/	/	45.3	49	36	8	7
#35	19.5	1.7	4.2	/	48.5	4.1	1.8	20.2	43	39	10	8
#36	32.4	3.6	5.9	/	1.9	7.8	1.5	46.9	/	83	9	8
#40	30.3	2.6	4.1	/	3.6	11.5	6.1	41.8	61	28	7	4
#43	26.8	3.1	5.6	/	3.2	4.8	10.9	45.6	46	34	10	10
#45	33.3	1.3	3.1	/	4.2	/	7.4	50.7	42	43	9	6
#50	45.6	3.7	4.6	/	/	/	5.0	41.1	26	52	12	10
#53	32.1	0.9	3.5	/	/	7	4.0	52.5	39	48	8	5
#58	41.5	0.9	3.8	/	0.9	3.7	0.5	48.7	27	63	5	5
#59	31.0	0.9	3.1	/	/	3.8	5.0	56.2	29	56	9	6
#61	40.2	2.1	6.4	/	/	7.2	7.3	36.8	33	43	12	12
#65	39.4	0.8	3.5		7.2	5.9	2.8	40.4	33	58	4	5
#127	29.2	5.7	12.6	/	/	/	1.4	51.1	59	26	6	9
#128	37.9	3.7	13.1		/	/	1.6	43.7	52	28	6	14
#129	40.7	4.3	12.8	2.9	/	/	1.8	37.5	50	27	6	17

resonance frequency of $\omega_0/2\pi = f_0 = 21.36$ MHz and is equipped with a 25 mm probe. All measurements were performed at a room temperature of approximately 25 °C.

(1) FID measurements

The FID measurements were conducted using the following acquisition parameters: a repetition time TW of 10 s, an instrument dead time τ_d of 17 μs, a data sampling interval τ_2 of 1 μs, and 983 acquisition points. Sufficient signal averaging was performed for each experiment, to ensure a signal-to-noise ratio (SNR) greater than 100.

The acquired FID data were processed using an inversion algorithm developed by the research team to obtain the T_2^* spectra. The inversion results were calibrated using a standard water sample and converted into equivalent water content per unit mass (in mg/g), allowing quantitative comparison with geochemical results.

(2) IR-CPMG and IR-FID measurements

In the IR-CPMG measurements, the inversion recovery delay time τ_3 in the T_1 recovery period was varied logarithmically from 58 μs to 10 s, with 28 different τ_3 values. In the T_2 decay period, the echo spacing (TE $= 2\tau_1$) was set to 0.1 ms, and 300 echoes were acquired. The T_1 recovery period in IR-FID measurements used the same τ_3 values as the IR-CPMG measurements. The T_2^* decay phase followed the same parameters as the one-dimensional FID measurements: $\tau_d = 17$ μs, $\tau_2 = 1$ μs, and 983 data points.

Both IR-CPMG and IR-FID measurements involved a sufficient number of signal accumulations to ensure an overall average SNR greater than 100. The acquired 2D data were subjected to inversion processing to yield T_1-T_2 spectra and T_1-T_2^* spectra, respectively. The signal amplitudes of both types of 2D spectra were calibrated using a standard water sample and converted to equivalent water content per unit mass of the sample, in mg/g.

3.3. *Geochemical analysis*

(1) TOC content analysis

TOC content was measured using a CS-i carbon–sulfur analyzer, following the GB/T19145-2003 standard. TOC reflects the total amount of organic carbon in the sample, including carbon present in hydrocarbons, bitumen, and kerogen. It is one of the commonly used indicators for evaluating organic matter abundance.

(2) Routine Rock-Eval pyrolysis

Routine Rock-Eval pyrolysis experiments were conducted using a Rock-Eval 6 instrument. Powder samples were first heated isothermally at 300 °C for 3 min to obtain the S_1 peak. The temperature was then ramped up to 650 °C at a rate of 25 °C/min to obtain the S_2 peak. Hydrocarbons released during the pyrolysis process were detected by a flame ionization detector and quantified based on calibration with a standard sample. The S_1 peak typically represents the content of free hydrocarbons, and the S_2 peak corresponds to the amount of cracking hydrocarbons generated from the thermal decomposition of heavy hydrocarbons, bitumen, and kerogen. The S_2 peak is a key geochemical indicator used to assess hydrocarbon generation potential and organic matter richness.

(3) Step-by-step (SBS) Rock-Eval pyrolysis

SBS Rock-Eval pyrolysis was also performed using a Rock-Eval 6 instrument. The detailed heating program was as follows. The sample was initially heated from 120 to 200 °C at a rate of 25 °C per minute and held at 200 °C for 3 min to obtain the $S_{1\text{-}1}$ peak. The temperature was then increased to 300 °C at the same heating rate and maintained for 3 min to acquire the $S_{1\text{-}2a}$ peak. Subsequently, the temperature was raised to 350 °C and held for 3 min to obtain the $S_{1\text{-}2b}$ peak. The heating continued to 450 °C, where the sample was again held for 3 min to generate the $S_{2\text{-}1}$ peak. Finally, the temperature was increased to 600 °C and maintained for 3 min to obtain the $S_{2\text{-}2}$ peak.

Fig. 4 illustrates the geochemical significance of the products released at different temperature stages during the SBS Rock-Eval experiment. A better understanding of the compositional characteristics of these fractionated pyrolysis products can be achieved by comparing their elution temperatures with the boiling points of *n*-alkanes within corresponding carbon number ranges.

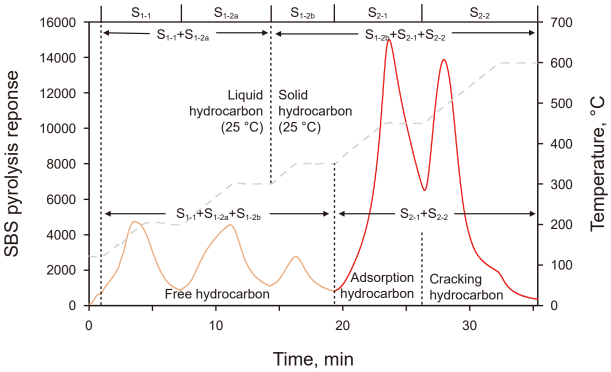

Fig. 4. Schematic diagram of products in different temperature ranges during step-by-step Rock-Eval pyrolysis experiments.

The $S_{1\text{-}1}$ peak primarily represents light molecular weight oil components with carbon numbers of 11 or less, such as *n*-undecane (n-$C_{11}H_{24}$), which has a boiling point of 196 °C. The subsequent $S_{1\text{-}2}$ peak represents light to medium molecular weight oil fractions and is further divided into the $S_{1\text{-}2a}$ and $S_{1\text{-}2b}$ sub-peaks. The $S_{1\text{-}2a}$ peak, observed between 200 and 300 °C, corresponds to compounds with carbon numbers ranging from 12 to 17, exemplified by *n*-heptadecane (n-$C_{17}H_{36}$), which boils at 302 °C. The $S_{1\text{-}2b}$ peak, appearing between 300 and 350 °C, is associated with compounds having carbon numbers between 18 and 20, such as *n*-eicosane (n-$C_{20}H_{42}$), with a boiling point of 342.7 °C. The $S_{2\text{-}1}$ peak, generated between 350 and 450 °C, mainly reflects heavier hydrocarbons and asphaltenes with carbon numbers in the range of 21–30. A typical example is *n*-triacontane (n-$C_{30}H_{62}$), which has a boiling point of 449.8 °C. Finally, the $S_{2\text{-}2}$ peak, formed between 450 and 600 °C, primarily indicates the thermal degradation products of kerogen. Some studies classify the $S_{1\text{-}1}$, $S_{1\text{-}2a}$, and $S_{1\text{-}2b}$ peaks as representing free hydrocarbons, the $S_{2\text{-}1}$ peak as adsorption hydrocarbons, and the $S_{2\text{-}2}$ peak as cracking hydrocarbons (Jiang et al., 2016; Zhang et al., 2020; Li et al., 2020).

Therefore, the parameter ($S_{2\text{-}1}$+$S_{2\text{-}2}$) represents the total amount of hydrocarbons generated from the thermal cracking of heavy hydrocarbons, bitumen, and kerogen. Its geochemical significance is consistent with the S_2 peak from routine Rock-Eval pyrolysis. However, the results obtained through step-by-step heating are less affected by the pyrolysis carry-over and confinement effect, leading to more precise outcomes. It is important to note the physical states of normal alkanes at the NMR measurement temperature (approximately 25 °C), considering that the NMR measurements in this study were conducted at this room temperature. Normal alkanes with carbon numbers of 17 or less, such as *n*-heptadecane (n-$C_{17}H_{36}$), are liquid at 25 °C, as its melting point is around 21 °C. In contrast, those with carbon numbers of 18 or greater, such as *n*-octadecane (n-$C_{18}H_{38}$), are solid, with melting points ranging from approximately 28 to 30 °C. Consequently, the parameter ($S_{1\text{-}2b}$ + $S_{2\text{-}1}$+$S_{2\text{-}2}$) signifies the total content of solid petroleum hydrocarbons, bitumen, and kerogen in the sample at NMR measurement temperature. This sum represents the total content of hydrocarbons existing in a solid state within the sample and can also serve as a key geochemical indicator for characterizing the SOM content of the sample.

4. Results and discussion

4.1. NMR measurements results

To illustrate the typical NMR responses observed across the sample set, the T_1-T_2 and T_1-T_2^* spectra of three representative shale samples (#45, #34 and #35), selected for their high, medium, and low SOM content, are shown in Fig. 5. The spectral peak regions were delineated in both spectra according to the distribution characteristics of each peak in Figs. 2 and 3. It can be observed that the T_1-T_2 and T_1-T_2^* spectra of the same sample exhibit consistent peak positions, with similar T_1 relaxation responses for peaks bearing the same labels. The primary differences lie in the transverse relaxation responses (T_2 and T_2^*). The T_2^* values of all hydrogen-bearing components are generally shorter than their T_2 counterparts. The contrast between different T_2^* values is also reduced, due to additional dephasing effects caused by magnetic field inhomogeneity and susceptibility contrast.

The $(T_1/T_2^*)/(T_1/T_2)$ ratios were calculated for five SOM-associated peaks across all 20 samples. The statistical distribution of these ratios is illustrated in Fig. 6. It can be seen that the $(T_1/T_2^*)/(T_1/T_2)$ ratios for peaks A, B, and D fall predominantly within the range of 1–25, whereas the ratios for peak C lie between 25 and 500. This observation supports the theoretical prediction in Section 2.4, indicating that SOM and hydrocarbons with low mobility exhibit significantly lower $(T_1/T_2^*)/(T_1/T_2)$ ratios compared to hydrocarbons with high mobility.

Peak H was frequently observed to exhibit two distinct behaviors across the 20 samples. For some samples, the $(T_1/T_2^*)/(T_1/T_2)$ ratio of peak H was high, similar to or significantly larger than that of peak C. This indicates the signal originates from gaseous hydrocarbons. These gas signals typically located in the region of $T_1 > 300$ ms and $T_2 > 1$ ms in the T_1-T_2 spectrum. For other samples, the ratio of peak H was approximately 1, which suggests the signal corresponds to a small fraction of SOM detectable by the IR-CPMG measurement. A few samples exhibited a ratio slightly less than 1, an inversion artifact caused by the overestimation of T_1 inherent to the limitations of the IR-CPMG T_1-T_2 measurement.

The total hydrogen content and the calculated SOM content for all these shale samples, obtained using different methods, are listed in Table 2. The hydrogen contents derived from T_1-T_2 spectra (ϕ_{t,T_1-T_2}) range from 15.66 to 39.86 mg/g. In contrast, the corresponding values from T_2^* spectra (ϕ_{t,T_2^*}) are much higher, ranging from 20.04 to 67.03 mg/g. The T_1-T_2-derived values represent only 33.83%–88.26% of those obtained from T_2^* measurements.

Although differences exist between the SOM contents estimated by Method I and Method II, both methods produce higher values than the direct T_1-T_2 estimates. The SOM content from Method I ($\phi_{\mathrm{OM,corr}}$) is approximately 1.55–6.23 times greater, and that from Method II ($\phi_{\mathrm{OM},T_1-T_2^*}$) is about 1.03–3.05 times greater than the corresponding values from T_1-T_2 analysis ($\phi_{\mathrm{OM},T_1-T_2}$). These results indicate that the IR-CPMG-based T_1-T_2 measurements suffer from significant signal loss due to their limited sensitivity to ultra-short relaxation components. The FID-based T_2^* and IR-FID-based T_1-T_2^* measurements are more effective in detecting such components and are therefore more reliable for quantitatively assessing ultra-short relaxation signals like SOM in shale oil reservoirs.

4.2. Geochemical analysis results

The TOC content and conventional Rock-Eval analysis results for these shale samples are presented in Table 3. The results show that the TOC content of the samples ranges from 0.64 wt% to 7.11 wt%. Samples #59 and #45 exhibit the highest TOC contents, at 7.11 wt% and 6.38 wt%, respectively. Samples #35 exhibit comparatively lower TOC contents of 0.64 wt%. Routine Rock-Eval pyrolysis results indicate that S_1 values range from 1.14 to 5.17 mg/g. The S_2 values range from 1.18 to 23.72 mg/g and are significantly higher than the S_1 values. These findings indicate substantial organic matter abundance across all these shale samples. In

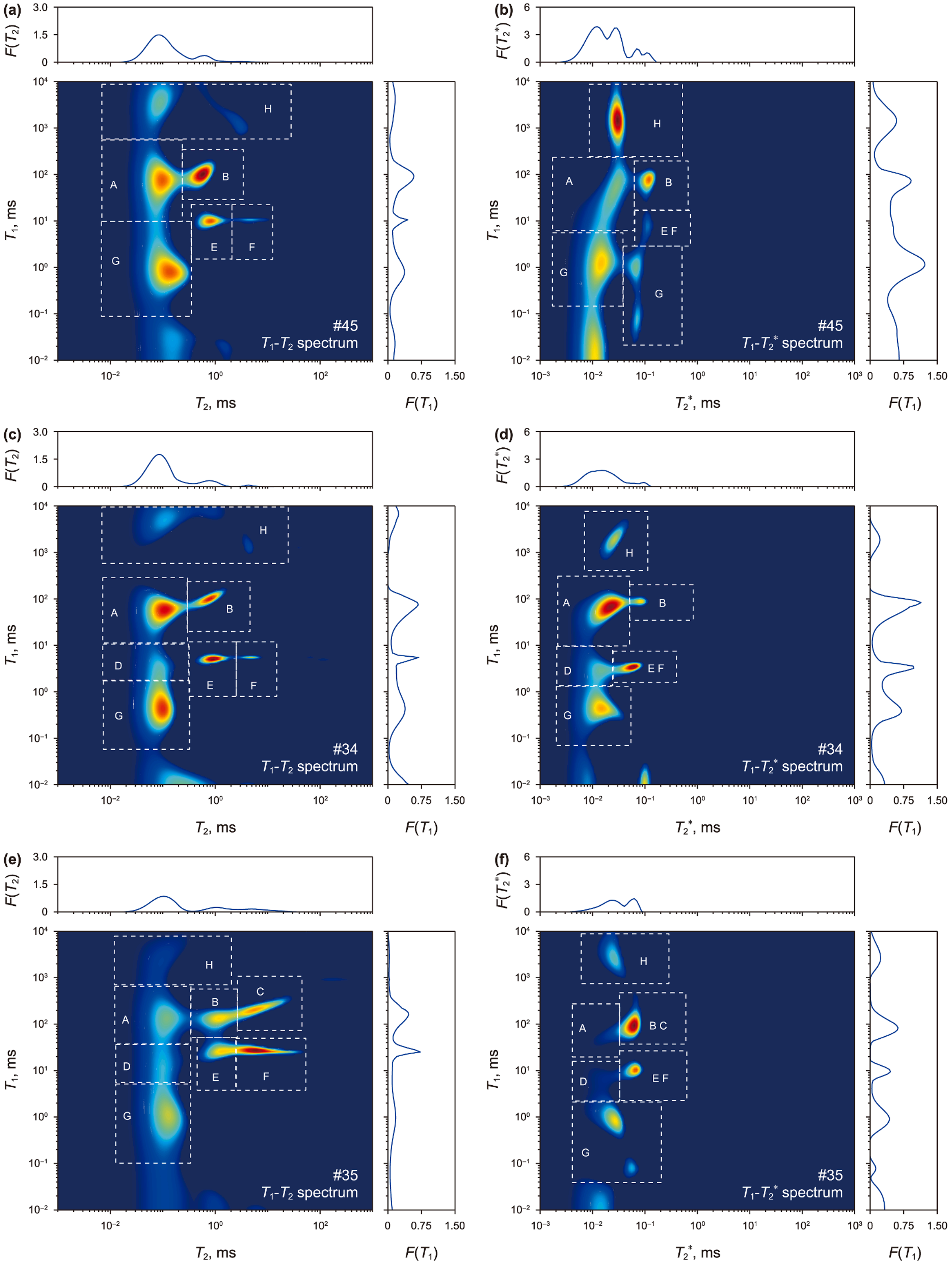

Fig. 5. Comparison of conventional T_1-T_2 spectra and the corresponding T_1-T_2^* spectra for three representative shale samples with high, medium, and low SOM content. The paired plots are for samples: **(a)** & **(b)** #45; **(c)** & **(d)** #34; **(e)** & **(f)** #35. For each pair, the left part is the T_1-T_2 spectrum and the right part is the T_1-T_2^* spectrum.

addition, heavy hydrocarbons, bitumen, and kerogen (S_2) account for a substantial proportion of the total hydrocarbon content (S_1+S_2), ranging from 50.86% to 86.41%. The T_{max} values range from 430 to 449 °C, indicating a moderate level of thermal maturity. As indicated in Table 2, all samples fall within the early oil window stage.

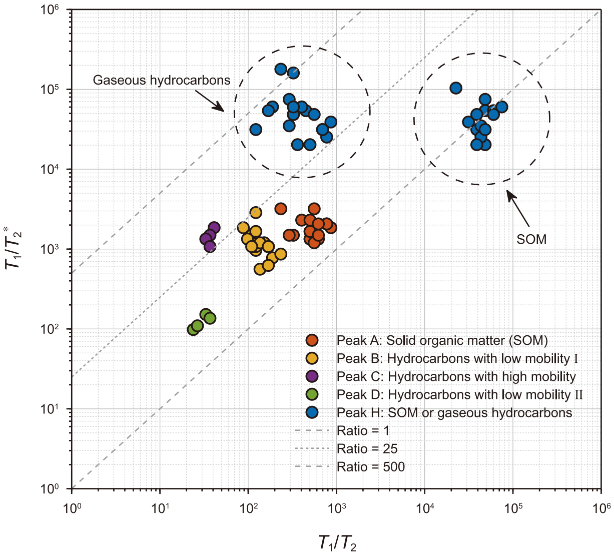

Fig. 6. Distribution of $(T_1/T_2^*)/(T_1/T_2)$ ratio for different hydrogen component peaks in shale samples.

Table 3
TOC contents analysis and routine Rock-Eval pyrolysis results for shale samples.

Sample ID	TOC, wt%	S_1, mg/g	S_2, mg/g	T_{max}, °C
#26	3.63	2.74	10.51	439
#28	4.49	3.67	10.24	442
#30	3.90	2.87	8.61	444
#31	4.40	3.37	9.86	441
#32	4.91	3.74	12.67	441
#34	3.81	3.29	9.09	447
#35	0.64	1.14	1.18	436
#36	5.50	3.26	14.21	446
#40	5.23	2.77	12.00	443
#43	4.50	2.84	9.36	445
#45	6.38	3.65	15.24	439
#50	5.44	2.98	15.31	443
#53	4.23	4.37	12.63	430
#58	4.44	3.95	13.98	440
#59	7.11	3.73	23.72	440
#61	5.24	4.00	14.84	445
#65	3.99	4.48	12.87	435
#127	4.78	3.87	15.22	449
#128	4.55	5.17	17.71	443
#129	4.09	3.84	13.95	447

Table 2
Solid organic matter (SOM) content calculated results based on method I and II for shale samples.

Sample ID	ϕ_{t,T_2^*}, mg/g	ϕ_{t,T_1-T_2}, mg/g	ϕ_{OM,T_1-T_2}, mg/g	$\phi_{OM,corr}$, mg/g	$\phi_{OM,T_1-T_2^*}$, mg/g
#26	46.07	26.72	8.21	27.56	13.60
#28	40.58	24.16	8.76	25.18	11.05
#30	48.24	28.66	11.07	30.65	11.62
#31	36.49	21.29	7.01	22.20	15.36
#32	42.80	23.02	8.34	28.12	16.21
#34	31.44	23.95	8.35	15.85	11.11
#35	20.04	15.66	3.09	7.47	3.95
#36	62.67	23.74	9.14	48.07	21.40
#40	48.44	21.47	8.37	35.33	14.87
#43	37.13	21.07	7.40	23.46	13.90
#45	67.03	22.68	8.47	52.82	21.53
#50	55.80	27.97	9.68	37.51	17.64
#53	50.73	27.28	5.40	28.85	14.36
#58	53.84	25.95	5.91	33.80	14.58
#59	59.99	27.47	7.77	40.29	23.42
#61	45.63	20.07	6.44	32.00	15.58
#65	39.84	25.75	4.74	18.82	14.47
#127	66.75	37.71	7.89	36.94	16.23
#128	48.86	38.18	11.52	22.19	11.95
#129	45.16	39.86	9.56	14.86	10.47

The SBS Rock-Eval pyrolysis analysis results for these shale samples are detailed in Table 4. Compared to routine Rock-Eval pyrolysis, the S_1 content ($S_{1\text{-}1}$+$S_{1\text{-}2a}$ + $S_{1\text{-}2b}$) obtained from SBS Rock-Eval pyrolysis ranges from 2.89 to 8.05 mg/g, approximately 1.13–2.53 times higher than conventional S_1 values. The S_2 content ($S_{2\text{-}1}$ + $S_{2\text{-}2}$) derived from this method ranges from 1.42 to 20.67 mg/g, comparable to S_2 values obtained through routine Rock-Eval pyrolysis. The cracking hydrocarbons ($S_{2\text{-}1}S_{2\text{-}2}$) accounts for approximately 32.95%–81.18% of the total hydrocarbon content ($S_{1\text{-}1}$+$S_{1\text{-}2a}$ + $S_{1\text{-}2b}$ + $S_{2\text{-}1}$ +$S_{2\text{-}2}$). The ($S_{1\text{-}2b}$ + $S_{2\text{-}1}$+$S_{2\text{-}2}$) content for these samples ranges from 1.94 to 21.94 mg/g, constituting approximately 45.01%–84.09% of the total hydrocarbon content. These findings suggest that hydrocarbons in the analyzed shale samples exist predominantly in a solid state under NMR experimental conditions.

4.3. Correlation analysis between NMR measurements and geochemical parameters

The correlation between the three SOM quantification methods and selected geochemical parameters is analyzed based on the previously discussed NMR measurements and geochemical data. Three methods are included in this analysis. The first is Method I (Method I: T_1-T_2&T_2^*), which is based on the T_1-T_2 spectrum and T_2^* spectrum difference correction. The second is Method II (Method II: T_1-T_2^*), which is based on the T_1-T_2^* spectrum. The third is the conventional method (Method: T_1-T_2) based on the T_1-T_2 spectrum. Four geochemical parameters capable of reflecting SOM content were selected for the correlation analysis: TOC, S_2 from routine Rock-Eval pyrolysis, ($S_{2\text{-}1}$+$S_{2\text{-}2}$) and ($S_{1\text{-}2b}$ + $S_{2\text{-}1}$+$S_{2\text{-}2}$) from SBS Rock-Eval pyrolysis. The quantitative accuracy of each method is

Table 4
Step-by-step (SBS) Rock-Eval pyrolysis results for shale samples. Note: The S_1 and S_2 values are calculated as $S_1 = S_{1\text{-}1} + S_{1\text{-}2a} + S_{1\text{-}2b}$ and $S_2 = S_{2\text{-}1} + S_{2\text{-}2}$.

Sample ID	$S_{1\text{-}1}$, mg/g	$S_{1\text{-}2a}$, mg/g	$S_{1\text{-}2b}$, mg/g	$S_{2\text{-}1}$, mg/g	$S_{2\text{-}2}$, mg/g	S_1, mg/g	S_2, mg/g	S_2+$S_{1\text{-}2b}$, mg/g
#26	2.01	1.97	0.99	7.20	5.36	4.97	12.56	13.55
#28	2.59	1.27	0.30	8.05	3.26	4.16	11.31	11.62
#30	2.06	1.59	0.42	6.92	2.57	4.07	9.49	9.91
#31	2.67	2.05	0.60	8.37	2.84	5.32	11.22	11.81
#32	3.07	1.85	0.46	9.80	4.31	5.38	14.11	14.57
#34	1.92	1.61	0.51	6.56	3.14	4.04	9.71	10.22
#35	1.19	1.18	0.52	0.96	0.46	2.89	1.42	1.94
#36	2.31	1.55	0.49	10.93	6.69	4.36	17.62	18.11
#40	2.54	1.89	0.64	10.46	4.44	5.07	14.90	15.54
#43	2.15	1.70	0.53	8.68	4.25	4.38	12.93	13.46
#45	2.90	2.89	1.49	11.79	8.58	7.28	20.37	21.86
#50	2.22	2.11	1.06	8.71	6.80	5.39	15.51	16.57
#53	2.59	3.22	1.63	8.31	3.91	7.44	12.22	13.85
#58	2.31	2.64	1.21	7.27	6.14	6.16	13.41	14.62
#59	2.09	2.06	1.27	11.80	8.87	5.42	20.67	21.94
#61	2.39	2.40	0.86	9.93	4.77	5.65	14.71	15.57
#65	2.89	3.48	1.68	8.88	4.16	8.05	13.04	14.72
#127	2.44	1.77	0.60	9.33	5.64	4.81	14.97	15.57
#128	2.63	3.38	1.33	7.76	5.94	7.34	13.70	15.03
#129	1.95	1.93	0.47	6.98	4.03	4.34	11.01	11.48

visually compared in the crossplots of Fig. 7(b)–(d), where the diagonal line represents a perfect agreement between the NMR-derived and Rock-Eval values.

The conventional T_1-T_2 method exhibits the weakest correlation with the four geochemical parameters. As shown in the figures, the gray circles are all located above the diagonal line, which confirms the fact that this method struggles to effectively capture signals from ultra-short relaxation components, leading to an underestimation of SOM content.

In comparison to the conventional T_1-T_2 method, the results from Method I show significantly improved correlations with all four geochemical parameters. It demonstrates great correlations with ($S_{2\text{-}1}$+$S_{2\text{-}2}$) and ($S_{1\text{-}2b} + S_{2\text{-}1}$+$S_{2\text{-}2}$), achieving high coefficients of determination (R^2) of 0.7176 and 0.6956 respectively. However, as illustrated in Fig. 7(b)–(d), the green data points for this method are all located below the diagonal line, indicating that the SOM values calculated by this method are systematically higher than the Rock Eval pyrolysis values. However, a key limitation of this method is its inability to distinguish the origin of these signals. Consequently, some liquid hydrocarbons with low-mobility and gaseous hydrocarbons are also counted in the SOM content, leading to an overestimation. This non-selective detection is precisely why Method I correlates so well with the S_2 parameter, as its content is also known to include these components.

The results from Method II also show markedly improved correlations with the four geochemical parameters compared to the other methods. It achieves a particularly high R^2 of 0.8828 with ($S_{1\text{-}2b} + S_{2\text{-}1}$+$S_{2\text{-}2}$) and the highest overall correlation with ($S_{2\text{-}1}$+ $S_{2\text{-}2}$), reaching an R^2 of 0.8958. As shown in Fig. 7(b)–(d), the corresponding yellow circles for this method are distributed near the diagonal line. This indicates that the SOM content obtained by this method is more consistent with the Rock-Eval results than the other two methods. This improved consistency is attributed to the mitigation of the overestimation issue inherent in Method I. It effectively excludes interference from liquid or gaseous hydrocarbon components by using T_1-dimensional information and a gas correction.

It can also be observed that the data for S_2 and ($S_{2\text{-}1}$+$S_{2\text{-}2}$) are systematically positioned below the diagonal line, although they are proximate to the diagonal line. This indicates that a slight overestimation by Method II relative to these parameters. In contrast, the data points for the ($S_{1\text{-}2b} + S_{2\text{-}1}$+$S_{2\text{-}2}$) parameter show excellent consistency. Most values fall directly on the diagonal. This excellent consistency indicates that the results obtained from Method II include the $S_{1\text{-}2b}$ component, which are medium molecular weight hydrocarbon fractions. These hydrocarbon fractions exist in a solid state at the NMR measurement temperature. Therefore, it is concluded that this method accurately quantifies the total sum of solid hydrogen components, including solid petroleum hydrocarbons, bitumen, and kerogen.

In conclusion, the two new methods proposed in this paper significantly improve the quantitative characterization of SOM. Method I provides a rapid estimation of total content of SOM but is prone to overestimation by including signals from liquid or gaseous hydrocarbon components. Method II successfully corrects for these interferences, accurately quantifying the total solid hydrogen content with results highly consistent with advanced Rock-Eval pyrolysis. Furthermore, both the proposed NMR-based methods offer clear practical advantages over the TOC content analysis and Rock-Eval pyrolysis. They are non-destructive, increase the sample volume nearly 600-fold from approximately 100 mg of powder to 60 g of core plug for enhanced representativeness, and eliminate complex, time-consuming procedures.

4.4. Discussion

This section discusses the applicability and limitations of the proposed methodology by examining the influence of two key factors pertinent to geological reservoirs: magnetic field inhomogeneity and temperature.

Magnetic field inhomogeneity is a critical factor for the NMR T_2^* relaxation analysis of shales. A primary source of such inhomogeneity in shales is the presence of paramagnetic minerals. The samples in this study contain pyrite, as shown in Table 1, which is a primary source of internal magnetic field gradients causing the signal of nearby hydrogen nuclei to decay rapidly. FID-based T_2^* measurements acquire data immediately following the instrument dead time, allowing for the characterization of such fast-relaxing signals. The strong consistency (Fig. 7(d)) demonstrates that the T_2^* measurement is effective for the shales in this study, which contain pyrite content up to 10.9 %. Furthermore, recent numerical simulations (Liu et al., 2025) also indicate that pyrite contents in the range of 1.51%–5.43% have a limited impact on the quantification of the SOM's T_2^* response. However, the FID

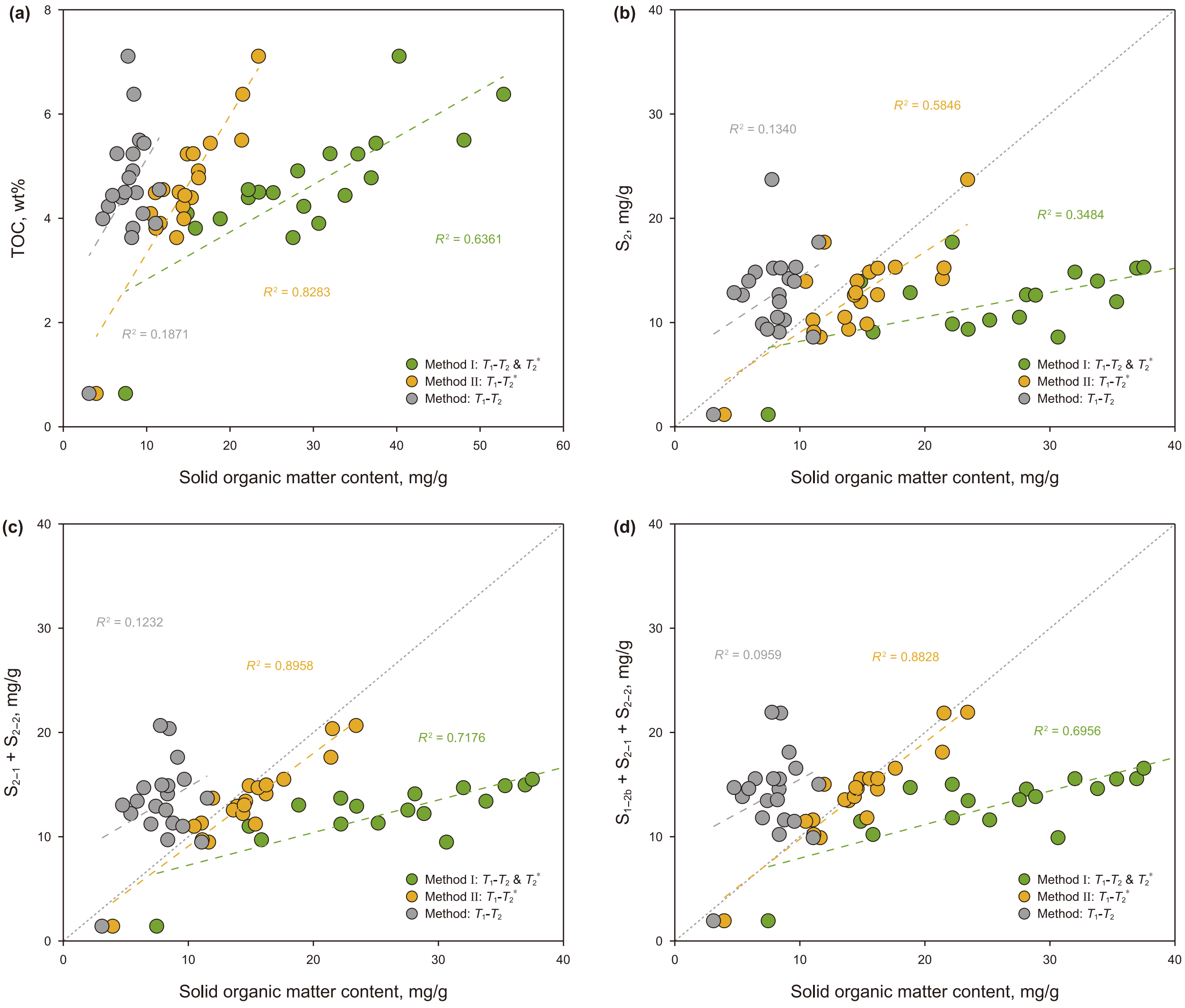

Fig. 7. Correlation analysis between organic matter content calculated by different NMR methods and geochemical parameters. The plots show correlations with **(a)** TOC, **(b)** the routine Rock-Eval pyrolysis parameter S_2, the sum of SBS pyrolysis parameters **(c)** $S_{2\text{-}1}$ + $S_{2\text{-}2}$, and **(d)** $S_{1\text{-}2}$ + $S_{2\text{-}1}$ + $S_{2\text{-}2}$.

measurements signal decay could become too rapid to be fully captured for shales with exceptionally high magnetic field inhomogeneity, which would potentially lead to an underestimation of SOM and pore fluid.

The NMR measurements in this work were conducted at an ambient temperature of 25 °C. The physical state of various hydrocarbon fractions aligns with the classification criteria for the geochemical parameter ($S_{1\text{-}2b}$ + $S_{2\text{-}1}$+$S_{2\text{-}2}$) at this temperature, which quantifies the solid hydrocarbon fraction under surface conditions. This allows for a direct comparison between the NMR-detected solid hydrogen signal and a geochemically defined solid hydrocarbon mass. It is well-established that increased molecular mobility leads to longer intrinsic T_1 and T_2 values at reservoir temperatures. This causes NMR signals to shift from a solid-like response ($T_2 \ll T_1$) towards a more liquid-like response ($T_1 \propto T_2$), a behavior that has been experimentally documented in analogous heavy hydrocarbon systems (Serve et al., 2021). Consequently, the SOM content quantified at 25 °C represents the total solid hydrocarbon resource at the surface, a portion of which transitions to a mobile liquid phase at reservoir conditions. However, the influence of temperature is different for T_2^* relaxation in shale. The T_2^* relaxation rate is the sum of the temperature-dependent intrinsic relaxation rate ($1/T_2$) and the temperature-independent contribution from magnetic field inhomogeneity. The T_2^* response is primarily controlled by magnetic field inhomogeneity for shale under the measurement conditions of this study. Consequently, the overall T_2^* relaxation is demonstrated to be remarkably insensitive to temperature changes, as the dominant contribution from magnetic field inhomogeneity is temperature-invariant. This inherent stability suggests that FID-based quantification methods are likely to be significantly more robust against temperature variations than conventional T_2-based measurements, representing a significant potential advantage for evaluating shale resources under diverse thermal regimes.

5. Conclusions

In this paper, FID and IR-FID pulse sequences were introduced to successfully address the limitations of conventional NMR measurements in shale oil reservoirs. Two novel methods are proposed for the quantitative characterization of SOM in shale reservoirs. The effectiveness of the proposed methods is systematically validated through a comparative analysis of the NMR-derived SOM content against key geochemical indicators. The specific conclusions are as follows.

1. Conventional IR-CPMG T_1-T_2 measurements are confirmed to severely underestimate shale resources, failing to capture over 13% of the total hydrogen signal. This is a direct result of the loss of ultra-short relaxation signals that the technique cannot detect.
2. Both newly proposed methods for SOM quantification vastly outperform the conventional T_1-T_2–based method. Method II, based on the T_1-T_2^* spectrum, consistently demonstrates the highest correlations with all selected geochemical parameters.
3. A novel parameter, the $(T_1/T_2^*)/(T_1/T_2)$ ratio, is established for the selective identification of SOM. This parameter provides a quantitative basis for distinguishing SOM, which typically exhibits a ratio of 1–25, from interfering signals such as gaseous hydrocarbons (ratio > 25).
4. Method II provides a non-destructive and accurate quantification of the total solid hydrocarbon content at the core scale, including solid petroleum hydrocarbons, bitumen, and kerogen. Its strong agreement with SBS Rock-Eval results validates its accuracy, while its larger sample scale and simpler analytical workflow offer significant practical advantages over traditional pyrolysis.

CRediT authorship contribution statement

Chen-Yu Xu: Writing – review & editing, Writing – original draft, Visualization, Validation, Software, Methodology, Investigation, Formal analysis, Data curation, Conceptualization. **Ran-Hong Xie:** Writing – review & editing, Supervision, Resources, Project administration, Methodology, Funding acquisition, Conceptualization. **Jiang-Feng Guo:** Writing – review & editing, Supervision, Resources, Methodology, Funding acquisition, Conceptualization. **Xiang-Yu Wang:** Visualization, Validation, Software, Data curation. **Li-Zhi Xiao:** Writing – review & editing, Supervision, Project administration. **Guo-Wen Jin:** Supervision, Validation, Writing – review & editing. **Bo-Chuan Jin:** Visualization, Validation, Software. **Xiao-Long Ju:** Validation, Software.

Declaration of interest

The authors declare that they have no known competing financial interests or personal relationships that could have appeared to influence the work reported in this paper.

Acknowledgements

This work was funded by the National Natural Science Foundation of China (42174131, 42304118, 42204107).

References

Enjileala, R., Guo, J., Macmillan, B., et al., 2021. T_1-T_2^* relaxation correlation measurements. J. Magn. Reson. 326, 106961. https://doi.org/10.1016/j.jmr.2021.106961.

Fleury, M., Romero-Sarmiento, M., 2016. Characterization of shales using T_1-T_2 NMR maps. J. Petrol. Sci. Eng. 137, 55–62. https://doi.org/10.1016/j.petrol.2015.11.006.

Gu, M., Xie, R., Jin, G., et al., 2021. Quantitative evaluation for fluid components on 2D NMR spectrum using Blind Source separation. J. Magn. Reson. 332, 107079. https://doi.org/10.1016/j.jmr.2021.107079.

Guo, J., Macmillan, B., Zamiri, M., et al., 2021a. Magnetic resonance T_1–T_2^* and $T_{1\rho}$–T_2^* relaxation correlation measurements in solid-like materials with non-exponential decays. J. Magn. Reson. 328, 107005. https://doi.org/10.1016/j.jmr.2021.107005.

Guo, J., Macmillan, B., Zamiri, M., et al., 2021b. Two dimensional ^{1}H magnetic resonance relaxometry-based analyses of Argonne premium coals. Fuel 302, 121106. https://doi.org/10.1016/j.fuel.2021.121106.

Guo, J., Zamiri, M., Balcom, B., 2022. Optimization of two-dimensional T_1^*–T_2^* relaxation correlation measurements in shale. J. Petrol. Sci. Eng. 217, 110939. https://doi.org/10.1016/j.petrol.2022.110939.

Hu, S., Zhao, W., Hou, L., et al., 2020. Development potential and technical strategy of continental shale oil in China. Petrol Explor Dev+ 47 (4), 877–887. https://doi.org/10.1016/S1876-3804(20)60103-3.

Jia, C., Zou, C., Yang, Z., et al., 2018a. Significant progress of continental petroleum geology theory in basins of Central and Western China. Petrol Explor Dev+ 45 (4), 573–588. https://doi.org/10.1016/S1876-3804(18)30064-8.

Jia, Z., Xiao, L., Chen, Z., et al., 2018b. Determining shale organic porosity and total organic carbon by combining spin echo, solid echo and magic echo. Micropor Mesopor Mat 269, 12–16. https://doi.org/10.1016/j.micromeso.2017.11.049.

Jiang, Q., Li, M., Qian, M., et al., 2016. Quantitative characterization of shale oil in different occurrence states and its application. Petroleum Geology & Experiment 38 (6), 842–849. https://doi.org/10.11781/sysydz201606842.

Jin, G., Xie, R., Xiao, L., 2020. Nuclear magnetic resonance characterization of petrophysical properties in tight sandstone reservoirs. J. Geophys. Res. Solid Earth 125 (2), e2019JB018716. https://doi.org/10.1029/2019JB018716.

Kausik, R., Fellah, K., Rylander, E., et al., 2016. NMR relaxometry in shale and implications for logging. Petrophysics 57 (4), 339–350.

Li, J., Jiang, C., Wang, M., et al., 2020. Adsorbed and free hydrocarbons in unconventional shale reservoir: A new insight from NMR T_1-T_2 maps. Mar. Petrol. Geol. 116, 104311. https://doi.org/10.1016/j.marpetgeo.2020.104311.

Liu, J., Xie, R., Guo, J., et al., 2025. Numerical Investigations on T_1-T_2^*-based Petrophysical Evaluation in Shale Oil Reservoir with Complex Minerals. PETROL SCI. Advance online publication. https://doi.org/10.1016/j.petsci.2025.07.020.

Liu, Y., Wang, X., Hirasaki, G., et al., 2023. Separation of solid and liquid components in organic-rich chalks using NMR relaxation. Fuel 333 (2), 126223. https://doi.org/10.1016/j.fuel.2022.126223.

Mitchell, J., 2014. Rapid measurements of heterogeneity in sandstones using low-field nuclear magnetic resonance. J. Magn. Reson. 240, 52–60. https://doi.org/10.1016/j.jmr.2014.01.006.

Mukhametdinova, A., Habina-Skrzyniarz, I., Krzyżak, A., 2021. NMR relaxometry interpretation of source rock liquid saturation— A holistic approach. Mar. Petrol. Geol. 132, 105165. https://doi.org/10.1016/j.marpetgeo.2021.105165.

Peters, K., 1986. Guidelines for evaluating petroleum source rock using programmed pyrolysis. AAPG Bull. 70 (3), 318–329. https://doi.org/10.1306/94885688-1704-11D7-8645000102C1865D.

Qian, M., Jiang, Q., Li, M., et al., 2017. Quantitative characterization of extractable organic matter in lacustrine shale with different occurrences. Petroleum Geology & Experiment 39 (2), 278–286. https://doi.org/10.11781/sysydz201702278.

Romero-Sarmiento, M., 2019. A quick analytical approach to estimate both free versus sorbed hydrocarbon contents in liquid-rich source rocks. AAPG Bull. 103 (9), 2031–2043. https://doi.org/10.1306/02151918152.

Rondeau-Mouro, Kovrlija, R., Van, S., et al., 2016. Two dimensional IR-FID-CPMG acquisition and adaptation of a maximum entropy reconstruction. J. Magn. Reson. 265, 16–24. https://doi.org/10.1016/j.jmr.2016.01.007.

Serve, O., Choblet, H., Livadaris, V., et al., 2021. Probing hydrocarbon dynamics at asphaltene/maltene interfaces for the global characterization of bitumen. J. Colloid Interface Sci. 593, 21–31. https://doi.org/10.1016/j.jcis.2021.02.076.

Silletta, E., Vila, G., Domene, E., et al., 2022. Organic matter detection in shale reservoirs using a novel pulse sequence for T_1-T_2 relaxation maps at 2 MHz. Fuel 312, 122863. https://doi.org/10.1016/j.fuel.2021.122863.

Song, Y., Kausik, R., 2019. NMR application in unconventional shale reservoirs–A new porous media research frontier. Prog. Nucl. Magn. Reson. Spectrosc. 112–113, 17–33. https://doi.org/10.1016/j.pnmrs.2019.03.002.

Washburn, K., Birdwell, J., 2014. Application of binomial-edited CPMG to shale characterization. J. Magn. Reson. 246, 72–78. https://doi.org/10.1016/j.jmr.2014.06.014.

Xie, X., Li, M., Littke, R., et al., 2016. Petrographic and geochemical characterization of microfacies in a lacustrine shale oil system in the Dongying Sag, Jiyang depression, Bohai Bay basin, eastern China. Int. J. Coal Geol. 165, 49–63. https://doi.org/10.1016/j.coal.2016.07.004.

Xu, C., Xie, R., Guo, J., et al., 2023. Comprehensive characterization of petrophysical properties in shale by solvent extraction experiments and 2D NMR. Fuel 335, 127070. https://doi.org/10.1016/j.fuel.2022.127070.

Xu, C., Xie, R., Wang, X., et al., 2024. A quantitative evaluation method for organic matter in shale based on CPMG and FID NMR experiments. Well Logging Technol. 48 (5), 574–585. https://doi.org/10.16489/j.issn.1004-1338.2024.05.002.

Yang, L., Jin, Z., 2019. Global shale oil development and prospects. China Petroleum Exploration 24 (5), 553–559. https://doi.org/10.3969/j.issn.1672-7703.2019.05.002.

Yang, Z., Zou, C., 2019. "Exploring petroleum inside source kitchen": Connotation and prospects of source rock oil and gas. Petrol Explor Dev+. 46 (1), 181–193. https://doi.org/10.1016/S1876-3804(19)30018-7.

Zamiri, M., Macmillan, B., Marica, F., et al., 2021. Petrophysical and geochemical evaluation of shales using magnetic resonance T_1-T_2^* relaxation correlation. Fuel 284, 119014. https://doi.org/10.1016/j.fuel.2020.119014.

Zamiri, M., Guo, J., Marica, F., et al., 2022. Characterization of kerogen in shale core plugs using T_2*-based magnetic resonance methods. Fuel 324 (A), 124573. https://doi.org/10.1016/j.fuel.2022.124573.

Zhang, H., Huang, H., Li, Z., et al., 2020. Comparative study between sequential solvent-extraction and multiple isothermal stages pyrolysis: a case study on Eocene Shahejie formation shales, Dongying depression, East China. Fuel 263, 116591. https://doi.org/10.1016/j.fuel.2019.116591.

Zhao, W., Hu, S., Hou, L., et al., 2020. Types and resource potential of continental shale oil in China and its boundary with tight oil. Petrol Explor Dev+. 47 (1), 1–11. https://doi.org/10.1016/S1876-3804(20)60001-5.

Zhao, W., Bian, C., Li, Y., et al., 2023. Organic matter transformation ratio, hydrocarbon expulsion efficiency and shale oil enrichment type in Chang 7_3 shale of Upper Triassic Yanchang Formation in Ordos Basin, NW China. Petrol Explor Dev+. 50 (1), 14–26. https://doi.org/10.11698/PED.20220459.

Zou, C., Yang, Z., Cui, J., et al., 2013. Formation mechanism, geological characteristics and development strategy of nonmarine shale oil in China. Petrol Explor Dev+ 40 (1), 15–27. https://doi.org/10.1016/S1876-3804(13)60002-6.

Zou, C., Pan, S., Jing, Z., et al., 2020. Shale oil and gas revolution and its impact. Acta Pet. Sin. 41 (1), 1–12. https://doi.org/10.7623/syxb202001001.

Zou, C., Ma, F., Pan, S., et al., 2023. Formation and distribution potential of global shale oil and the developments of continental shale oil theory and technology in China. Earth Sci. Front. 30 (1), 128–142. https://doi.org/10.13745/j.esf.sf.2022.8.29.